Case Studies in Construction Materials 17 (2022) e01622

Contents lists available at ScienceDirect

Case Studies in Construction Materials

journal homepage: www.elsevier.com/locate/cscm

Experimental study of temperature effect on the mechanical tensile fatigue of hydrated lime modified asphalt concrete and case application for the analysis of climatic effect on constructed pavement

Qinghua Wei [a], Azedin Al Ashaibi [b], Yu Wang [b,*], Amjad Albayati [c], Jonathan Haynes [b]

[a] School of Civil Engineering, Chongqing Jiaotong University, Chongqing China
[b] School of Science, Engineering & Environment, University of Salford, Manchester M5 4WT, UK
[c] Department of Civil Engineering, University of Baghdad, Iraq

ARTICLE INFO

Keywords:
Asphalt pavements
Hydrated lime additive
Thermal stress
Fatigue Analysis

ABSTRACT

Previous experimental studies have suggested that hot mixed asphalt (HMA) concrete using hydrated lime (HL) to partially replace the conventional limestone dust filler at 2.5% by the total weight of all aggregates showed an optimum improvement on several key mechanical properties, fatigue life span and moisture susceptibility. However, so far, the knowledge of the thermal response of the modified asphalt concrete and thermal influence on the durability of the pavement constructed are still relatively limited but important to inform pavement design. This paper, at first, reports an experimental study of the tensile fatigue life of HMA concrete mixes designed for wearing layer application. Tests were conducted under three different temperatures for five mixes of different HL contents and one with no use of HL. On the experimental data, temperature effect on material fatigue was characterized in terms of the S-N curve modelling parameters. At last, numerical modelling, set at a climatic scenario in the UK, was performed to analyse and compare the seasonal climatic thermal influence on the fatigue life of two pavement structures using and not using the HL modified HMA concrete. Both the experiment and modelling have demonstrated that the 2.5% HL HMA concrete largely enhances the fatigue life of the material and the constructed pavement.

1. Introduction

Climate change and economic sustainability have posed big challenges for road infrastructure. Directly exposed to atmosphere and traffic, pavement surfaces subject to a prominent combined deteriorating mechanism caused by the coupled traffic loading, atmospheric and surrounding environmental temperature variation, and direct solar radiation [1,2], for which the fatigue deterioration is the most common form. Modifying asphalt concrete using mineral additives as a micro-filler has been widely adopted and proves to be effective to improve flexible pavement durability. Among the varied functional mineral additives, hydrated lime (HL) has been, for

* Corresponding author.
E-mail address: y.wang@salford.ac.uk (Y. Wang).

https://doi.org/10.1016/j.cscm.2022.e01622
Received 3 September 2022; Received in revised form 24 October 2022; Accepted 27 October 2022
Available online 28 October 2022

some time, of particular interest due to its outstanding effectiveness, wide availability, and economical cost [3,4].

Although many experimental studies have reported significant improvement in the mechanical properties of asphalt mixes using HL additive [5,6] and the optimum rate of addition [7], so far, few experimental studies have been undertaken for the temperature influence on the fatigue life of HL modified asphalt concrete [8–10]. Meanwhile there has been little reported work on computational analysis for the climatic thermal impact on the fatigue life of pavement structures constructed using the HL modified asphalt concrete [11–15]. As an effort to increase the knowledge in these aspects, a series of experiments have been performed. A previous publication [16] has reported experimental tests for thermal properties of asphalt concrete with and without HL modification, and numerical modelling which compared thermomechanical response of the pavement structures using the two materials, respectively, when exposed to an environmental temperature condition. This paper reports a continuation of the experimental study to compare the tensile fatigue life of the hot mixed asphalt (HMA) concrete with and without the use of HL additive. The concrete mix is designed for the wearing surface layer application. The tests were conducted under three different temperatures. The experimental data establish a characterization model for the temperature effect on the tensile fatigue life of the HMA concrete. To demonstrate its practical meaning, a numerical modelling was performed to analyse the stress and strain status of a pavement structure exposed to traffic loading and environment impact. Different a previous modelling work [16], in this paper,. set at a geo-climatic scenario, the modelling refers to a real climatic condition by taking into account the direct solar radiation to illustrate a practical meaning case investigation of the coupled thermomechanical conditions on the pavements using and without using HL. In line with previous study, the work contributes new data and knowledge of the material and applications.

2. Experiment of temperature effect on tensile fatigue life

An experiment was performed to study the temperature effect on six different mixes designed for wearing course application following the Standard for Road and Bridge Construction [17]. A control mix used limestone dust for the mineral filler by 7% of the total weight of aggregates. The five other mixes used HL to replace the limestone dust in the control mix at a rate of 1 %, 1.5 %, 2 %, 2.5 % and 3 %, respectively, by the total weight of aggregates. All the mixes were cast into beams of a dimension of 76 (W) × 76 (D) × 381 (L) mm. These beam specimens were then tested for their fatigue life using the four-point bending method [18] at three temperatures, i.e., 15 °C, 20 °C and 25 °C, and four loads, i.e., 223, 310, 402, and 490 N, respectively. The loads were cyclic at 2 Hz frequency. They were in a rectangular form with 0.1 s of loading followed by 0.4 s without loading. In each test, the tensile strain (ε_{t_200th}) of the bottom surface of the beams at the middle span position was recorded at the 200th repetition and taken as the initial applied strain for the S-N curve measurement. Further information about the mix design, sample preparation, experimental setup and test procedure, etc. has been detailed in a previous work in the same laboratory of this work [19].

Fig. 1 shows the temperature effect on the measured strain at the 200th cycle under the four applied loads. The control mix displaces the lowest initial strain at temperature 15 °C & 25 °C, but nearly the higest at 20 °C. However, the 2.5 % HL mix is just opposite, with the highest initial strain at 15 °C & 25 °C, but the lowest one at 20 °C. Such little correlation between the initial strain and temperature may be explained due to the initial microstructure adjustment of the mixes under fresh state. However, generally, the 2.5 % HL mix shows about the lowest strain at all three temperatures at the highest load, 490 N.

Fig. 2 shows the fatigue test results, the S-N curves. It can be seen from Fig. 2(b), showing a linear trend at the log-log scale, the mix of 2.5 % HL at the three temperatures has the smallest slope. Meanwhile, at the same initial strain, the 2.5 % HL mix has the highest load repetition number (N_f) before failure at temperature 25 °C, and at other two temperatures, 15 °C & 20 °C, and when the initial stain is less than 270 micro-strain. The result has confirmed and strengthened the conclusion in other previous studies [16,19,20] that 2.5 % HL addition can be an optimum rate for HMA concrete to obtain a compromised material property improvement when exposed

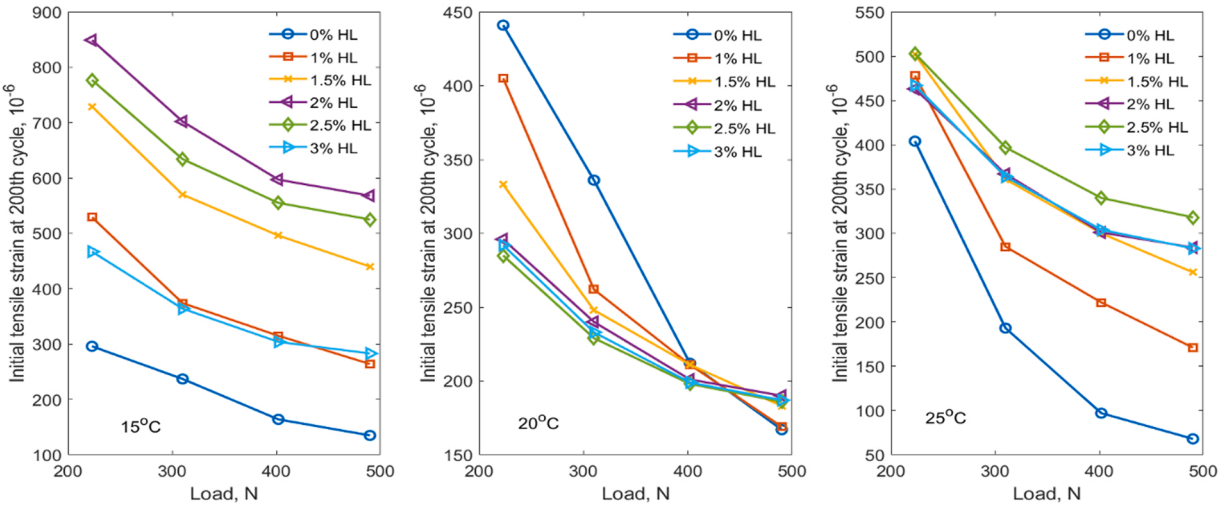

Fig. 1. The initial strain at 200th cycles loading vs the loads applied.

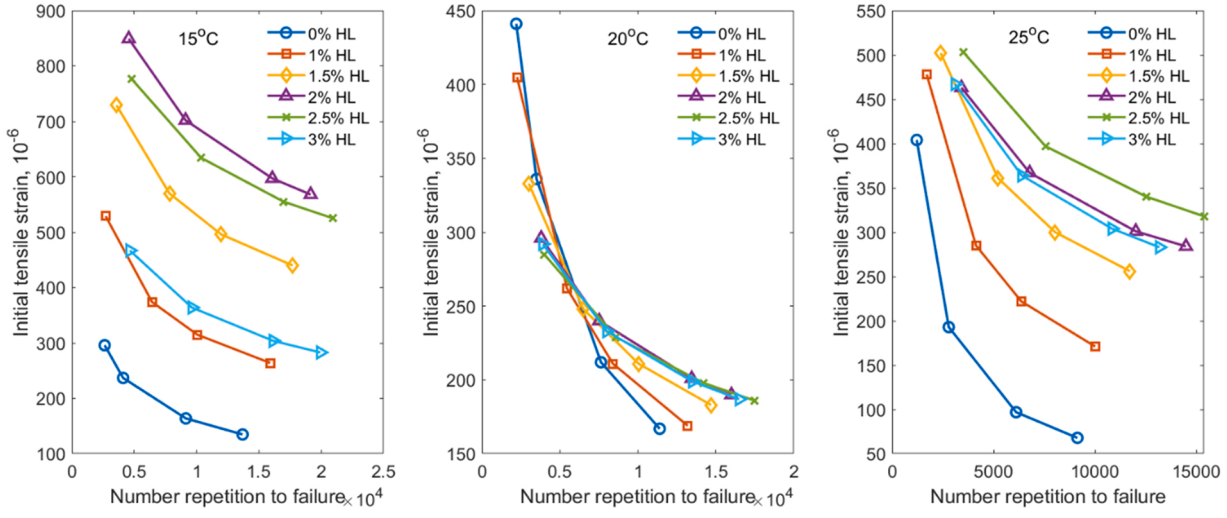

(a) in normal scale

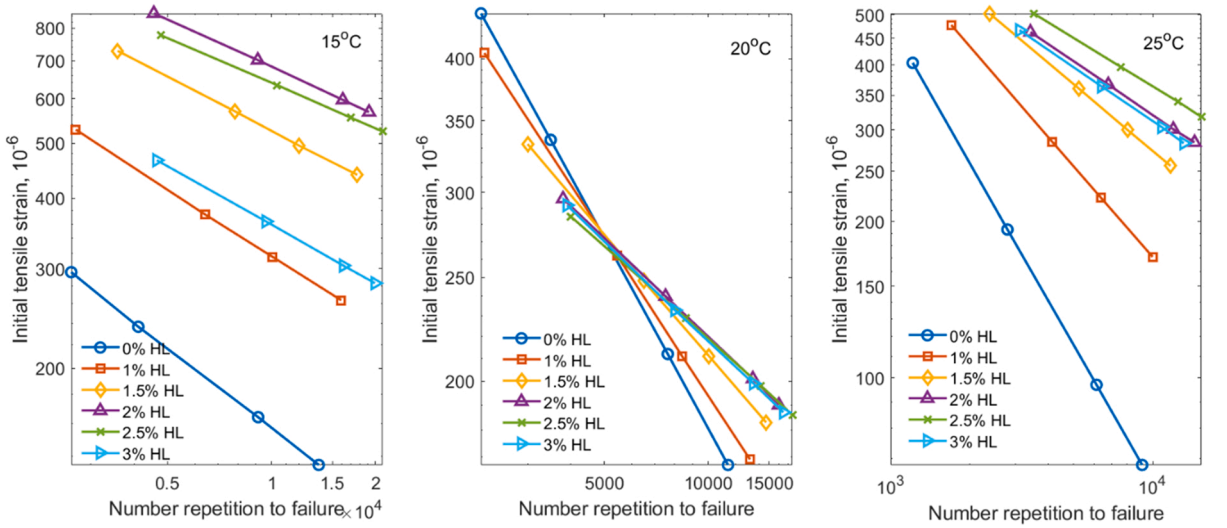

(b) in log-log scale

Fig. 2. Fatigue test results of the 6 mixes for wearing course application.

to both mechanical loading and thermal influence.

Fig. 3 highlights a comparison of the results for the mix of 2.5 % HL and the control mix (0 % HL) shown in Fig. 2. A power function, $\varepsilon_{t\_200th} = k_1 N_f^{k_2}$, which is generally used to represent the S-N curves of materials, has been adopted to fit the data. The fitting results are shown in the log-log scale presentation, which demonstrate a good representation.

Fig. 4 plots the obtained two fitting parameters, k_1 and k_2, data against temperature, where the relation between the two parameters and temperature is well represented using two polynomials, from which temperature effect on the S-N curve of the wearing mixes of 0 % and 2.5 % HL addition can be written into the form of Eq. (1):

- For 0% HL addition:

$$\varepsilon_{t\_200th} = \left(2.83 \times 10^{-3} T^2 \quad - \quad 9.30 \times 10^{-2} T \quad + \quad 0.77\right) N_f^{\left(-4.09 \times 10^{-2} T + 0.17\right)} \tag{1a}$$

- For 2.5% HL addition:

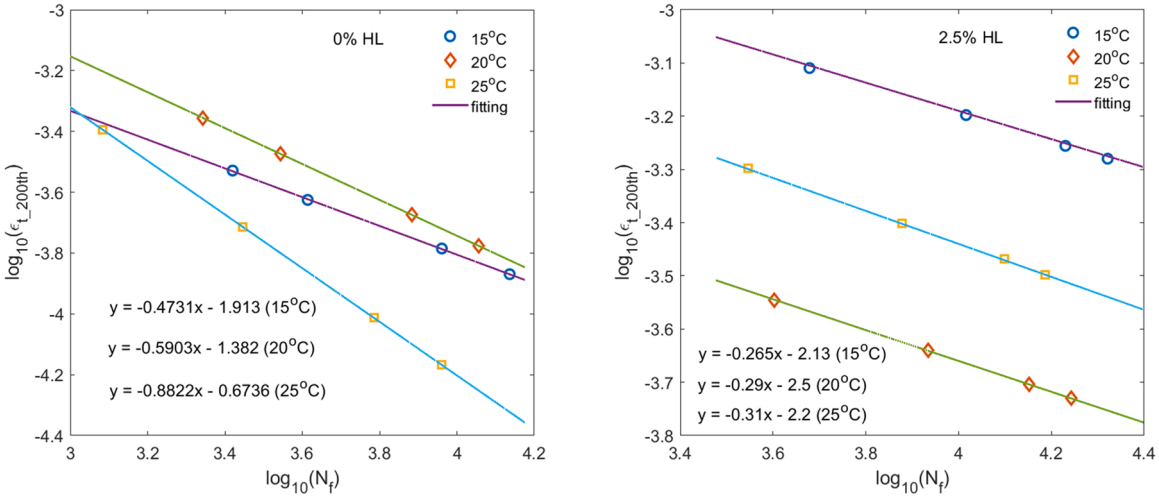

Fig. 3. The S-N curve of the mix of 2.5 % HL under three temperatures and the fitting at log-log scale.

$$\varepsilon_{t\_200th} = \left(1.48 \times 10^{-4} T^2 \quad - \quad 6.03 \times 10^{-3} T \quad + \quad 6.46 \times 10^{-2}\right) N_f^{\left(-4.50 \times 10^{-3} T - 0.20\right)} \tag{1b}$$

where ε_{t_200th} is the strain recorded at 200th repetition, T is the temperature in℃, N_f is the fatigue life - the maximum repetition number of a certain strain before failure.

The plots demonstrate that in the case of 2.5 %HL the average absolute value of k2 in the range of temperatures is much less than that in the case of 0 %HL. It means that the S-N curve of the mix of 2.5 %HL is much flatter than that of the mix of 0 %HL in the log-log scale. Therefore, under the same stress condition the mix of 2.5 %HL has a higher fatigue life in the range of temperature variation. The mechanism improving fatigue resistance is due to the high porosity and chemical reactivity of HL particles. The high porosity enhances the contact surface between the mineral filler and the asphalt cement particles, which make the mixes have higher density and stiffness. The chemical reactivity improves the bitumen–aggregate adhesion [21] and slows down bitumen aging [22] because of the pozzolanic reaction activated by the HL.

3. Modelling the coupled thermomechanical effects on pavement structures

3.1. Governing equations

A classical thermomechanical model [23] is adopted to describe the coupled thermomechanical effect on pavement structures and to compare the predicted fatigue life for the pavements using the asphalt concrete of 0 % and 2.5 % HL addition, respectively.

- **Motion equation**

For an isotropic solid material, its deformation follows the Navier's equations, which can be written in the form below:

$$\frac{E}{2(1+\nu)}\left(\frac{1}{(1-2\nu)}\nabla(\nabla \bullet \mathbf{u}) + \nabla^2 \mathbf{u}\right) + \mathbf{f} = \rho \frac{\partial^2 \mathbf{u}}{\partial t^2} \tag{2},$$

where $\mathbf{u}$ stands for the vector of displacement in space (u_x u_y u_z), $\mathbf{f}$ is a body force per unit volume, E is modulus and ν is Poisson ratio, ρ is density. The strain and stress of solid materials are:

$$\varepsilon_{ij} = \frac{1}{2}\left(\frac{\partial u_i}{\partial x_j} + \frac{\partial u_j}{\partial x_i}\right) \tag{3},$$

$$\sigma_{ij} = \lambda \varepsilon_{kk} \delta_{ij} + 2\mu \varepsilon_{ij} - \alpha(3\lambda + 2\mu)\Delta T \delta_{ij} \tag{4},$$

where $\lambda = \frac{\nu E}{(1-2\nu)(1-2\nu)}$ and $\mu = \frac{E}{2(1+\nu)}$ are the Lamé parameters; α is the thermal expansion/contraction coefficient; ΔT is the temperature change. For a static loading condition, the term on the right-hand side will disappear as $\frac{\partial^2 \boldsymbol{u}}{\partial t^2} = 0$.

- **Energy equation**

The thermal energy conservation of solid materials follows the Eq. (5):

$$\rho C_p \frac{dT}{dt} = \nabla(k \nabla T) + \rho \dot{r} - \alpha(3\lambda + 2\mu) T \frac{d\varepsilon_{kk}}{dt} \tag{5},$$

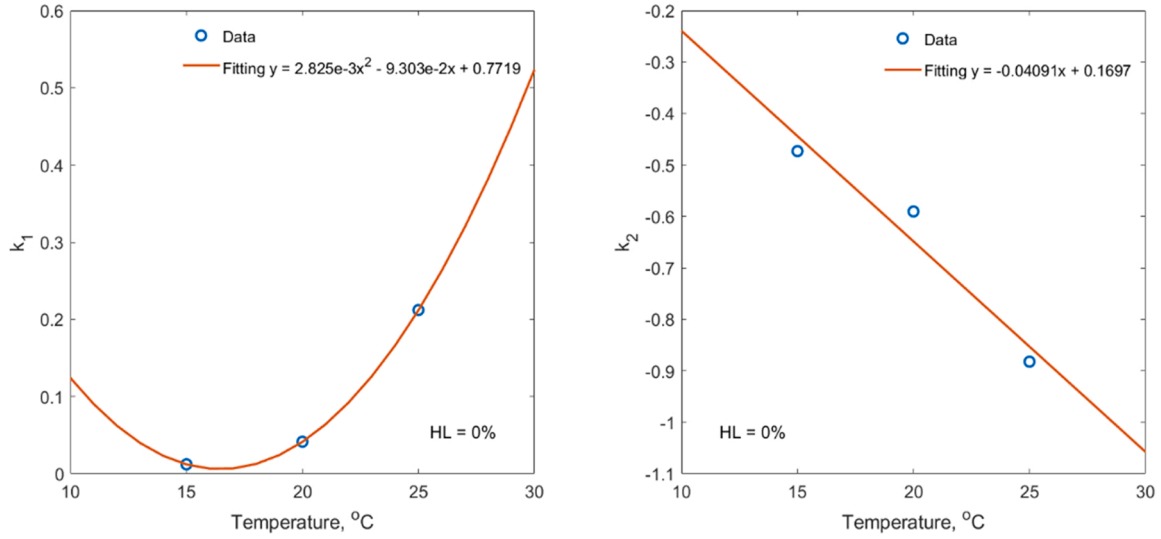

(a) 0% HL

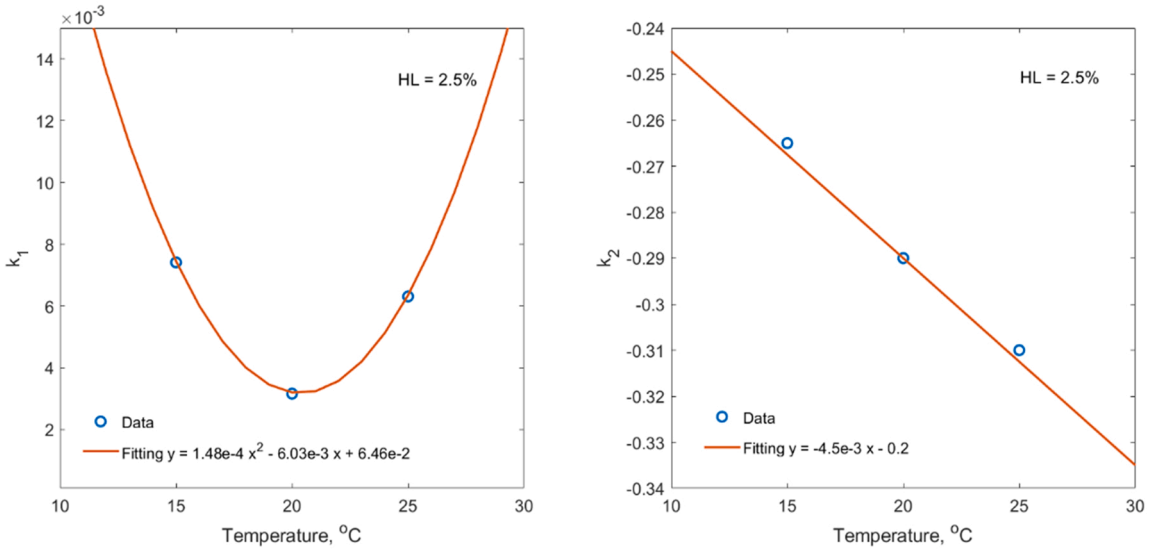

(b) 2.5% HL

Fig. 4. Characterization of the k_1 and k_2 variation with temperature.

where C_p is specific heat, k is thermal conductivity, $\dot{r}$ is heat source per unit mass. The last term stands for the deformation rate ($\frac{d\varepsilon_{ik}}{dt}$) energy, which is too small to be neglectable for the current thermal effect problem only.

3.2. *Material properties*

Solving the system of the Eqs. (2)–(5) needs the materials' physical, thermal and mechanical properties, and their variation at different temperatures. Table 1 gives the relevant properties for the asphalt concrete mixes of 0% and 2.5% HL addition, which are primarily from a previous study conducted at the same research laboratory [16,21]. But for the thermal deformation coefficient, a model based on a laboratory study on a newly constructed asphalt pavement [24] was adopted, which used two quadratic polynomials in the form of the Eq. (6) to estimate the coefficients of thermal expansion (CTE) and contraction (CTC) for their variation with temperature.

$$CTC = \quad -1.62\times10^{-8}T^2 + 9.46\times10^{-7}T + 1.75\times10^{-5} \tag{6a}$$

Table 1
Material properties of pavement materials.

Property	HL content	Pavement layer				
		Wearing	Levelling	Base	Subbase	Subgrade
Modulus E (MPa)	0 %	$0.28\,T^2 - 41.53\,T + 2090$	$0.39\,T^2 - 46.41\,T + 1929$	$0.34\,T^2 - 40.41\,T + 1649$	170	65
	2.5 %	$0.19\,T^2 - 43.03\,T + 2623$	$0.52\,T^2 - 63.3\,T + 2527$	$0.34\,T^2 - 41.12\,T + 1803$		
Poisson ratio u	0 %	0.35			0.4	
	2.5 %					
Density ρ (g/cm^3)	0 %	2.34	2.32	2.31	1.76	1.29
	2.5 %	2.32	2.30	2.30		
Thermal Conductivity k (W/m/K)	0 %	0.72	0.73	0.75	1.3	0.28
	2.5 %	0.90	0.78	0.88	1.3	0.28
Thermal Capacity c_p (J/kg/K)	0 %	1062.6	1092.79	1121.12	837	800
	2.5 %	1333.48	1155.49	1303.09	837	800
Thermal deformation coefficient α	0 %	CTE			3.32×10^{-6}	3.4×10^{-5}
	2.5 %	CTC				

$$CTE = \quad 4.34 \times 10^{-9} T^2 - 2.34 \times 10^{-7} T + 2.78 \times 10^{-5} \tag{6b}$$

The data for the two foundation layers (subbase and subgrade) are from other published work [25].

4. Modelling the climatic thermal effect on a pavement structure

4.1. A pavement finite element model

A single lane carriageway pavement structure of five layers was modelled using finite element (FE) method. The coupled thermomechanical model of the Eqs. (2)–(5) was implemented using the partial differential equation module of the software COMSOL Multiphysics. Fig. 5 shows half of the symmetric pavement structure. A wheel represents the traffic. Table 2 lists the geometric information.

4.2. Climatic thermal conditions

The thermal interaction between pavement and local atmospheric environment has been a topic of interest in pavement engineering and urban environment research. The thermal exchange at the pavement surface consists of three physical mechanisms, i.e., the solar irradiation adsorption, pavement emission and interfacial air convection [4,14,15], which decide the vertical thermal flux at

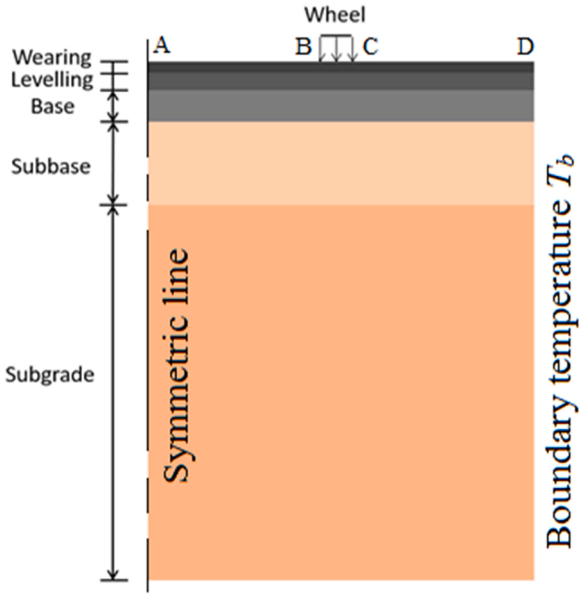

Fig. 5. FE geometric model (A, B, C & D are four positions on pavement surface).

Table 2
FE geometric data.

	Wearing	Levelling	Base	Subbase	Subgrade	Wheel
Depth (mm)	50	70	90	300	2500	–
Width (mm)	1800	1800	1800	1800	1800	250

the pavement surface, which can be described using the Eq. (7):

$$q_T = (1-a)I - \varepsilon\sigma\left(T_s^4 - T_a^4\right) - h_c(T_s - T_a) \tag{7}$$

where q_T (W/m^2) stands for the vertical thermal flux at the pavement surface, a is the albedo coefficient of the pavement material, I (W/m^2) is the solar incident irradiation, ε is pavement material emissivity, σ is the Stefan-Boltzmann constant, 5.67×10^{-8} W/m^2/K^4, h_c (W/m^2/K) is the heat convection coefficient.

For the climatic thermal effect analysis, this paper differs from a previous study [16] which used an assumed temperature condition. By setting a scenario at a location in Greater Manchester, in northwest England, a database of the UK Global Horizontal Irradiance (GHI) [26] has been referenced to determine a more realistic thermal boundary condition for the FE modelling of the pavement structure. The GHI database records the annual hourly incident irradiation around the UK. To characterise these data for the FE modelling parametric input, at first, an average daily variation by hours in each month was calculated. Fig. 6 gives the result of the data at the location set up (GHI_tmy_MIDAS X_394936,Y_392020 2008_2017 [27]. A Gaussian distribution (Eq. 8) is employed to represent the average hourly GHI in a day for each month in a period of one year. Thereafter, the three representative Gaussian parameters, a, b and c are characterized for their monthly variation using a sum sine function as given out in the Fig. 7.

$$GHI = a \times \exp\left(-\left(\frac{t-b}{c}\right)^2\right) \tag{8}$$

where t is the time in hours, a, b and c are three parameter constants.

To determine the q_T by the Eq. (7), we still need to know the atmospheric air temperature T_a, for which the data from UK weather forecast record is adopted here. Fig. 8(a) shows the annual monthly temperature variation in the region of Manchester and a representative curve fitting to the average of the Low and High. Fig. 8(b) shows the variation of amplitude - the difference between the Average and the Low or High, and a representative curve fitting to the data of the amplitude. On the data and the representatives in Fig. 8, the hourly atmospheric air temperature is characterised using the Eq. (9). Fig. 9 illustrates the modelled temperature condition during one year.

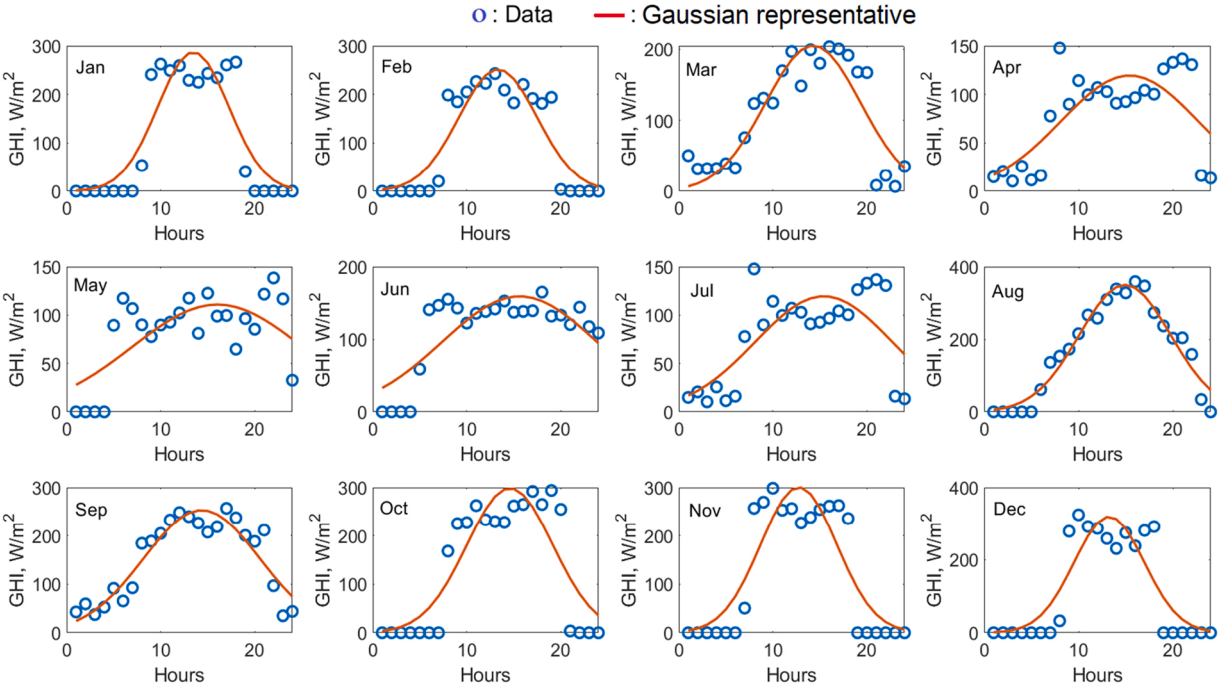

Fig. 6. Annual monthly average daily Global Horizontal Irradiance in hours at the location in Greater Manchester UK.

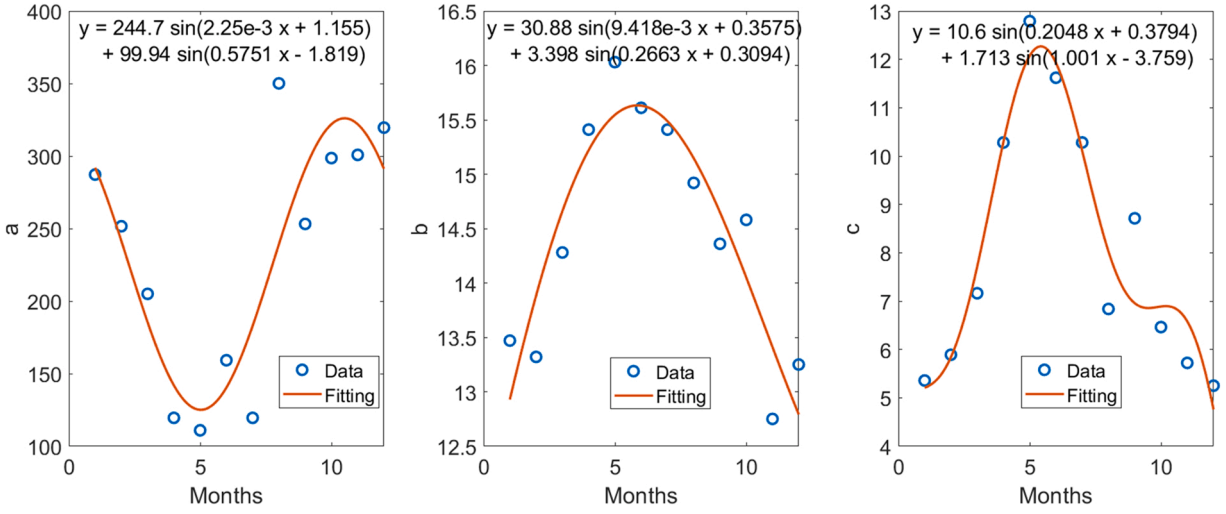

Fig. 7. Characterized Gaussian representative parameters.

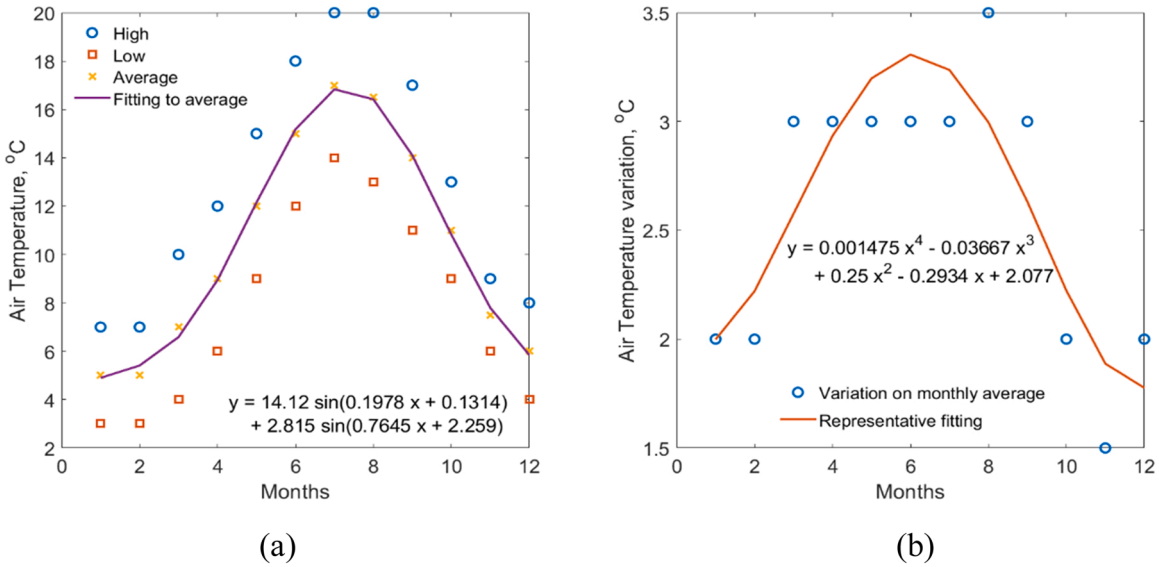

Fig. 8. UK Manchester area annual temperature variation.

$$T_a = \quad T_{mean} + DT \times \sin(2\pi t/24) \tag{9}$$

where T_{mean} is the average curve in the Fig. 7(a), and $DT = \frac{High-Low}{2}$ is the variation magnitude against the average and represented by the curve in the Fig. 7(b), t is the time in hours. The x in both Fig. 7(a)&(b) is the time in months, i.e., $x = t/30/24$.

A number of heat convection models have been proposed for h_c in Eq. (7) [15]. h_c directly relates to the local atmospheric weather state, such as temperature, humidity and wind [28,29]. As it is not a key topic of this paper, a constant value, 13.5 W/m^2/°C, a data according to [30], was assumed.

To solve the energy equation, Eq. (5), the thermal boundary condition must be defined. A thermal insulation condition is applied at the symmetric line. For the boundary temperature T_b, a geological survey of the shallow ground seasonal temperature in the UK [31] is assumed for the surrounding ground condition for this work. Fig. 10(a) shows the data and characterization fitting curves for the temperature variation at five depths underground, i.e., 0, − 0.5, − 1, − 2 and − 3 m. Fig. 10(b) shows a left boundary temperature at 720hrs, 2880hrs, 5040hrs and 7200hrs. An initial temperature condition in the structure is assumed to be 10 °C, referring the mean value at the depth − 0.5 m.

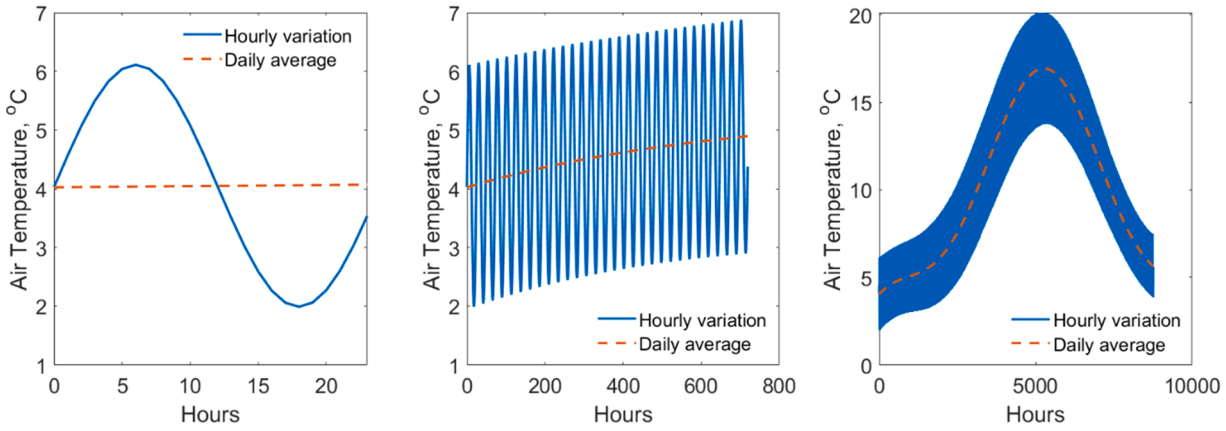

Fig. 9. Characterized hourly air temperature variation in one year time.

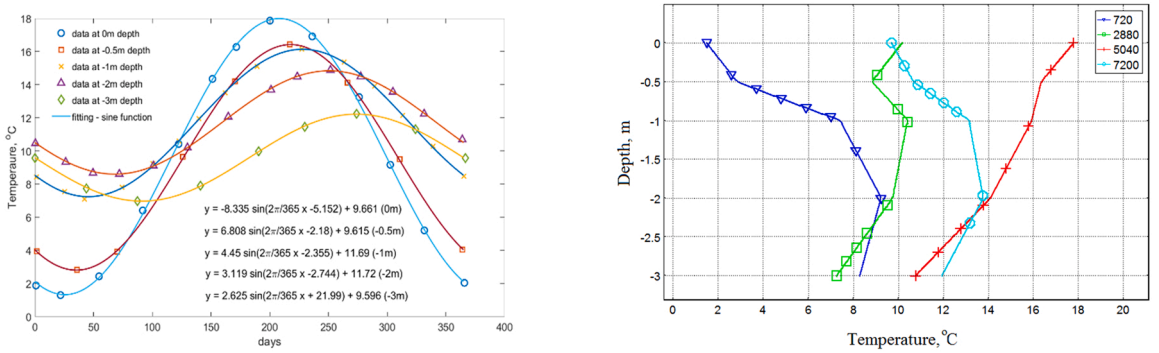

(a) Year-round UK shallow ground temperature variation [31]

(b) Vertical temperature profile at the right side

Fig. 10. Temperature boundary condition.

4.3. Traffic condition

A wheel pressure applied on the surface represents the traffic loading. An equivalent single wheel load of 70 kN [16] is set for the modelling work, which gives a wheel load pressure of 0.772 MPa on an estimated contact area of 9.073×10^{-2} m^2 [19]. The boundary condition to solve the motion equation, Eq. (2), assumes that there is no horizontal displacement for the vertical edges of all layers, and no vertical displacement at the bottom of the subgrade.

5. Modelling results

- **Temperature, Deformation and Strain**

Fig. 11 shows the calculated pavement surface temperature variation at the four positions A, B, C & D in Fig. 5. It can be seen that the surface hourly temperature variation is almost identical for the two mixes, which has the biggest variation amplitude at the edge of the pavement. The surface temperature presents a similar patten to the atmospheric air temperature shown in Fig. 9. The calculated annual average surface temperature is 10.3 °C at the positions |A, B, and C, and 9.8 °C at D for both pavements. The annual maximum temperature, at position A, B & C, is about 1.5 °C lower but at position D is about 2 °C higher than that of the atmospheric air shown in Fig. 9. The predicted local surface temperature variation justifies the informative advance of the thermal boundary condition adopted by this paper compared to the previous study [16] which used a uniform pavement surface temperature condition.

Fig. 12 compares the vertical deformation at the pavement surface at four different seasonal times in a year (720 hrs in February (Winter), 2880 hrs in May (Spring), 5040 hrs in August (Summer), 7200 hrs in November (Autumn)). It can be seen that the pavement using 2.5 % HL addition has up to 1 % less deformation at the position bearing traffic loading. The result is similar to that predicated based on assumed surface temperature condition [16]. In addition, both of the boundary conditions are in agreement that the biggest

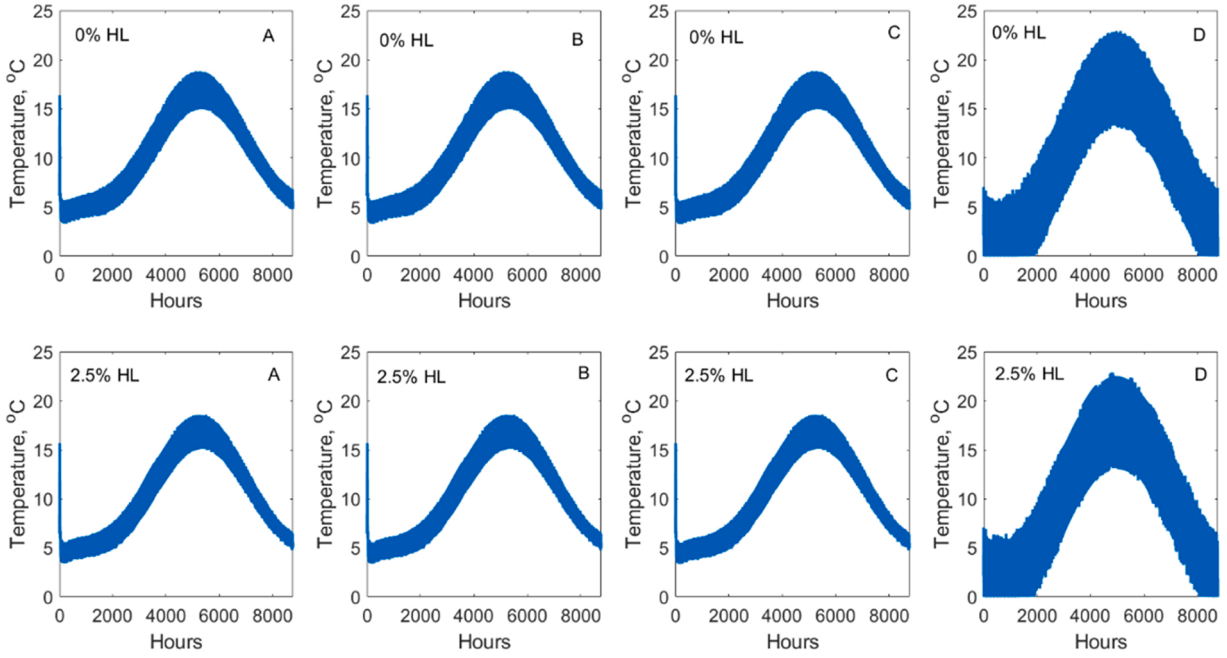

Fig. 11. Pavement surface temperature variation in a year.

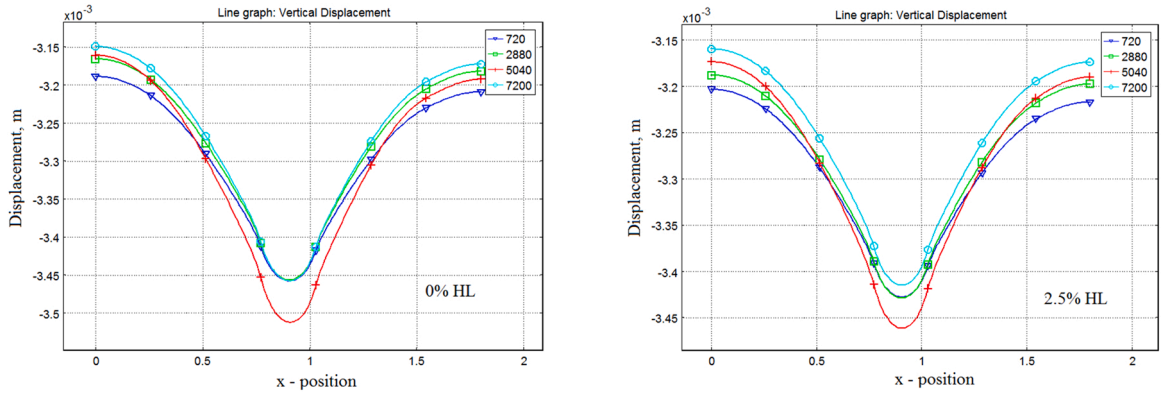

Fig. 12. Comparison of the vertical deformation of pavement surface.

vertical deformation at surface happened in the Summer time (5040 hrs). However, compared with the vertical displacement prediction in [16], Fig. 12 here shows a much smaller difference of the vertical displacement in the other seasons, i.e., Winter, Spring and Autumn. The result highlights the importance of accurate boundary condition description.

Fig. 13 illustrates the vertical temperature profile of the pavement structure at position A at a time in four seasons. It shows that, in a year-round time, the biggest temperature variation is at the surface. The seasonal temperature variation decreases downward, the vertical temperature profiles of the HL pavement and that using no HL are very close with very small difference, less than 0.5 °C, at surface. Based on the result, the rest of the study will primarily focus discussion on the surface layer of the pavement. The results of Fig. 13 are also closely similar to that predicted using temperature boundary condition [16].

Fig. 14 compares the maximum thermal strain and the two principal mechanical strains due to traffic load only in the pavement structure across a year. It shows that the annual maximum thermal strain ($\varepsilon_t = \alpha\Delta T$) profiles of the pavements using HL much higher than that of no use of HL. The maximum difference is about 100 times. The maximum 1st principal mechanical strain ($\varepsilon_{max} = \frac{\varepsilon_{xx}+\varepsilon_{yy}}{2} + \sqrt{\left(\frac{\varepsilon_{xx}-\varepsilon_{yy}}{2}\right)^2 + \left(\varepsilon_{xy}\right)^2}$) is in tension (positive), which is higher than thermal strain in the 0% HL pavement, but much lower than the thermal strain in 2.5%HL pavement. Meanwhile it shows that the 2nd principal strain ($\varepsilon_{min} = \frac{\varepsilon_{xx}+\varepsilon_{yy}}{2} - \sqrt{\left(\frac{\varepsilon_{xx}-\varepsilon_{yy}}{2}\right)^2 + \left(\varepsilon_{xy}\right)^2}$) in the pavements is very small and is in compression (negative). For the reason, this paper only discusses the coupled effect of the thermal strain and the 1st principal mechanical strain based on the assumption that the tensile strain plays the principal role in fatigue cracking

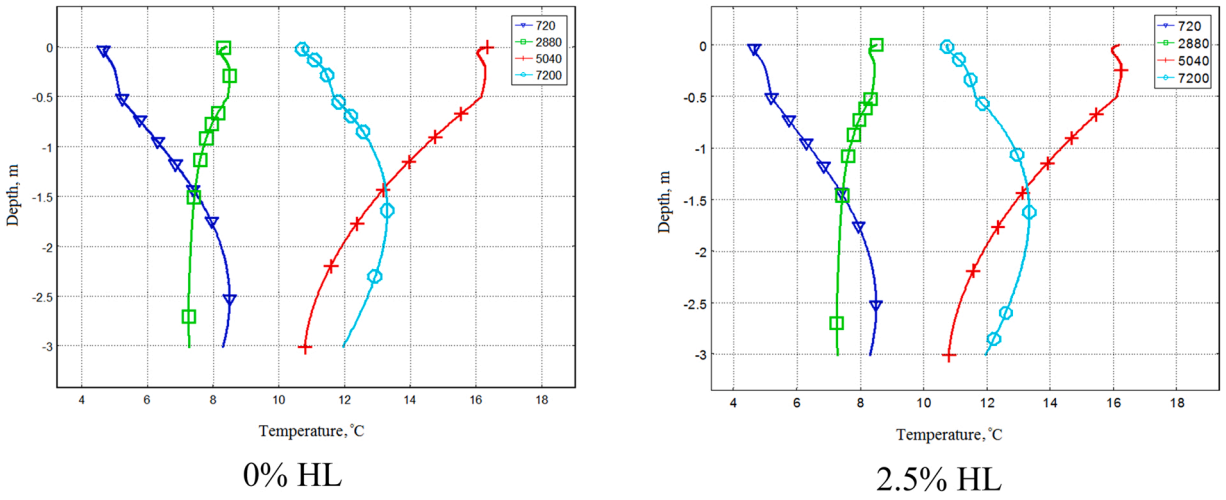

Fig. 13. Pavement vertical temperature at position A.

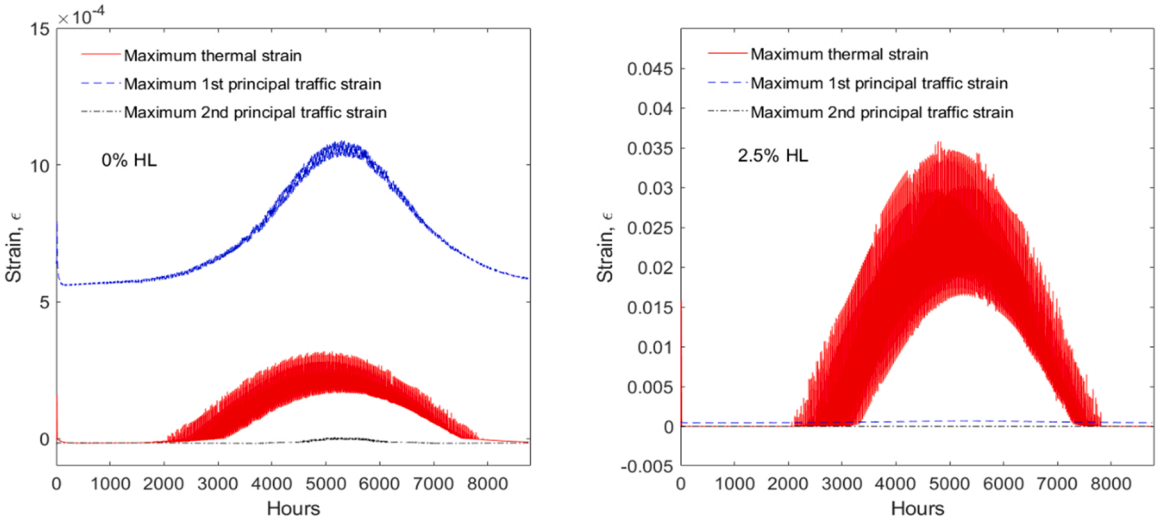

Fig. 14. The maximum thermal strain and mechanical strain in pavement structure.

of pavement.

Fig. 15 compares the hourly variation of the thermal strain and 1st principal mechanical strain of pavement surface at four positions (A, B, C and D in Fig. 5) across a year. Fig. 15(a) shows that the HL pavement has a much higher thermal strain at surface than the pavement using no HL in the two warm seasons, spring and summer (3000–7000 hrs). The coupled resultant strain, which is defined as $\varepsilon_{max} - \varepsilon_T$ in term of the Eq. (4), in this period, is also high but in compression for the HL pavement. Fig. 15(b) highlights the tensile states in the time of a year. It is not a surprise that the highest value is at the position directly bearing traffic (B & C), where the local tensile stress level in 2.5 % HL pavement is lower than that in the 0 %HL by 13 % and more. Particularly, in summer, the whole surface strain state is in compression for the pavement of 2.5 %HL. The result indicates that pavement is exposed to the most severe condition in winter. The annual average coupled resultant strains are, 3.99×10^{-5}, 1.897×10^{-4}, 1.851×10^{-4}, 5.82×10^{-5}, at A, B, C and D, for 2.5 %HL pavement, and are 3.99×10^{-5}, 3.738×10^{-4}, 3.575×10^{-4}, 5.81×10^{-5} for 0%HL pavement. At the positions B and C, the annual average of 2.5 %HL pavement is about 50 % lower than that of 0 %HL.

- **Pavement Fatigue life Estimation in Terms of Tensile Stress**

The fatigue life of asphalt pavement not only depends on the cyclic traffic loading and temperature, but also the thermal variation history of the asphalt binder [32]. A parameter of complex modulus, $G^*sin\delta$, is used as the criteria for the fatigue of asphalt binder, which however has received considerable criticism. For the reason, a time sweep using the dynamic shear (DSR) has been proposed [33]. For asphalt concrete mixtures specifically, a D^R failure criterion has also been proposed [34]. The variable D^R is defined as the

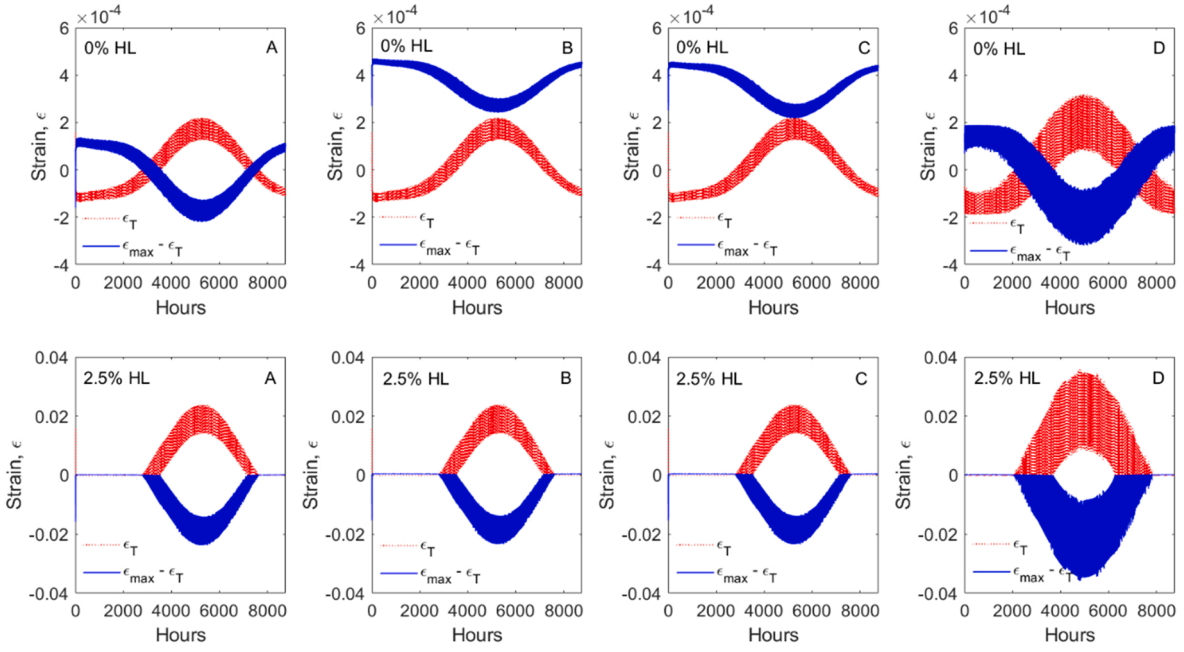

(a) The thermal strain, ε_T and the coupled strain, $\varepsilon_{max} - \varepsilon_T$

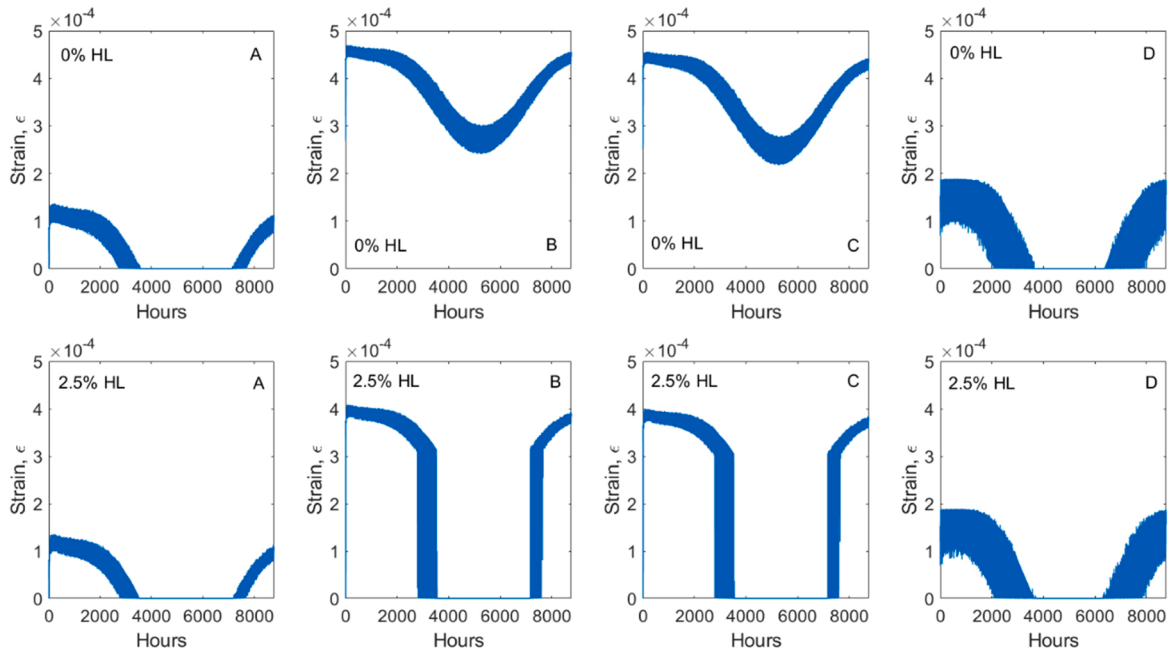

(b) The coupled strain in tensile state, $\varepsilon_{max} - \varepsilon_{T>=0}$

Fig. 15. The coupling of thermal & 1st principal mechanical strain at pavement surface.

average loss of integrity per cycle throughout service life of asphalt mixture. The higher the D^R value the greater the ductility of the asphalt mixture [34]. As the main purpose is to compare the HL effect, this paper simply uses the structural strain information and the result of the tensile fatigue tests to evaluate the fatigue life of pavement under coupled climatic and traffic conditions. Using a classical linear cumulative-damage theory (or the Palmgren-Miner rule), a rate of fatigue life consumed or loss is defined as:

$$R_f = \sum_{i=1}^{k} \frac{n_i}{N_f(\varepsilon_i)} \tag{10}$$

where $N_f(\varepsilon_i)$ stands for the fatigue life of the material subjected to a stain ε_i under the load i, k is the total number of different loads applied, and n_i is number of the cycle of each respective load i. The value of N_f is estimated using Eq. (1), where the ε_{t_200th} simply takes the value of the coupled resultant stain, i.e., $\varepsilon_t = \varepsilon_{max} - \varepsilon_T$. By this method, the rate of fatigue life consumed in the period of a year can be approximated by integrating the $1/N_f$ curves obtained. Since the temperature variation is in a daily cycle, the fatigue life is simply evaluated based on the daily average values of the surface temperature and the coupled resultant strain at position B. Fig. 16 shows

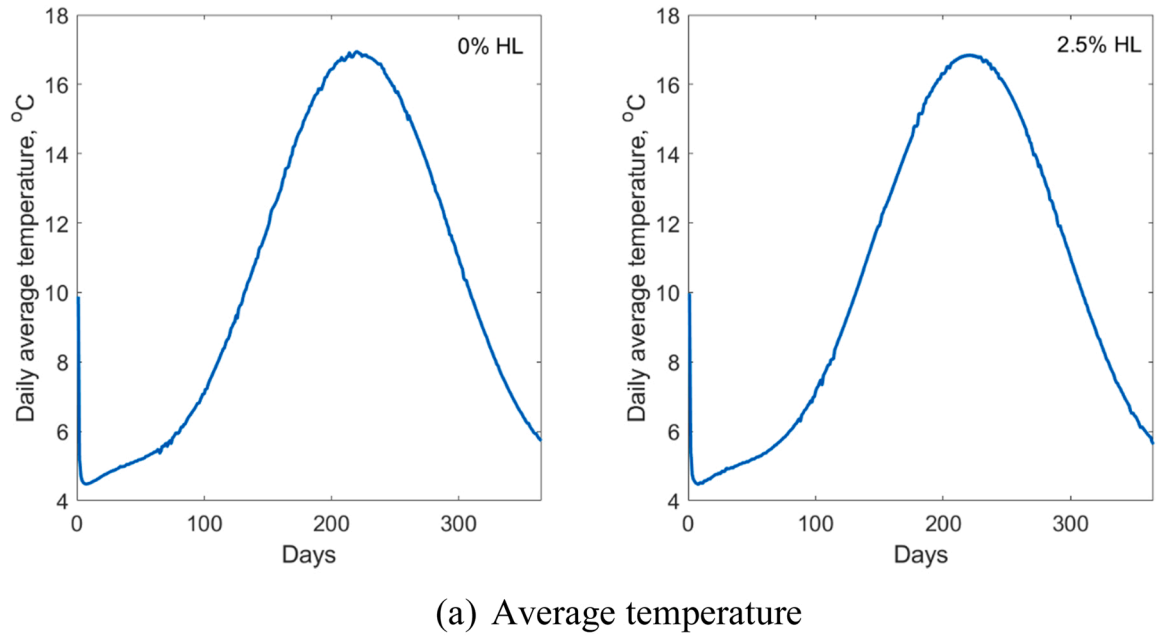

(a) Average temperature

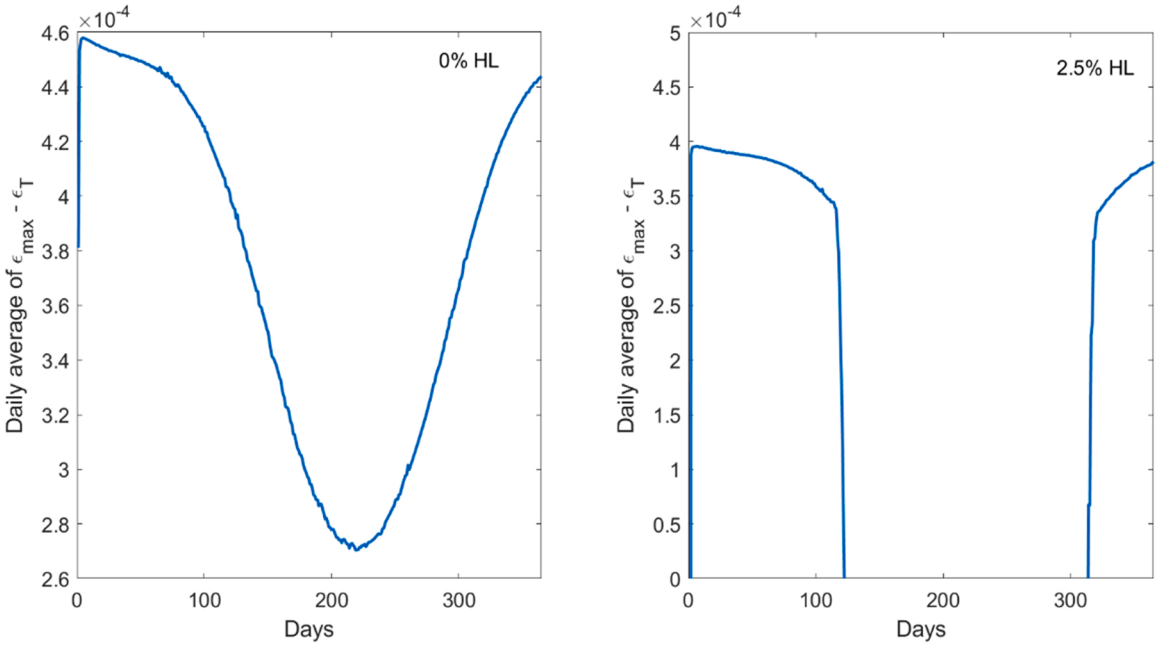

(b) Average tensile strain

Fig. 16. The daily average of the surface temperature and the coupled resultant strain at position B.

their average value by days, which only shows the tensile strain, as compressive strain is considered to have simply negligible effect on fatigue in this paper, which referring to a bending test.

Fig. 17 shows the calculated the $1/N_f$ at the position B on the pavement surface using the Eq. (1) and the daily data in Fig. 16. We can see that the pavement using the 2.5% HL asphalt concrete has a much lower fatigue life consumption that the pavement using the concrete with no HL modification. Fig. 17(a) illustrates that the main fatigue life consumption for 0% HL pavement would be under hot temperature in summer, while 17(b) illustrates that the 2.5% HL pavement has the major fatigue life consumption under cold temperature in late autumn and winter. Comparing with the surface deformation result in Fig. 12, an interesting finding is that the highest fatigue consumption and the largest deformation happen in opposite seasonal temperature conditions for the pavement using HL. Overall, the modelling analysis further confirms that HL asphalt concrete has outstanding improvement on pavement performance exposed to coupled thermomechanical loading.

6. Conclusion

This paper presents an experimental study of temperature effect on the fatigue life of asphalt concrete mixes using hydrated lime for partial mineral filler. A case study of numerical modelling has been performed to estimate the seasonal climatic effect on the constructed pavement and the benefit of the hydrated lime asphalt concrete. From the study, the following conclusion can be drawn:

- The reported experiment has confirmed that the 2.5% replacement of the conventional limestone filler using hydrated lime will generate an optimum increment of the fatigue life for the wearing course mix under three different temperatures. The result and conclusion are in line with what found in the study of other mechanical properties.
- The case study of numerical modelling highlights the advance of the heat transfer boundary condition over a temperature boundary to give more informative prediction.
- The modelling results illustrate an interesting finding that the pavements using and not using HL modified asphalt concrete have quite different thermomechanical strain states in different seasons. HL modified pavement has a higher rate of fatigue life loss under cold condition, such as in winter, however, the pavement using no HL has a higher fatigue life loss under hot condition, such as in summer.
- For pavement using HL, the largest deformation and the highest fatigue consumption happen in opposite different climatic seasons.
- In line with the material experiment, the modelling has further confirmed that HL asphalt concrete has outstanding improvement on pavement durability exposed to coupled thermomechanical loading.

Declaration of Competing Interest

The authors declare that they have no known competing financial interests or personal relationships that could have appeared to influence the work reported in this paper.

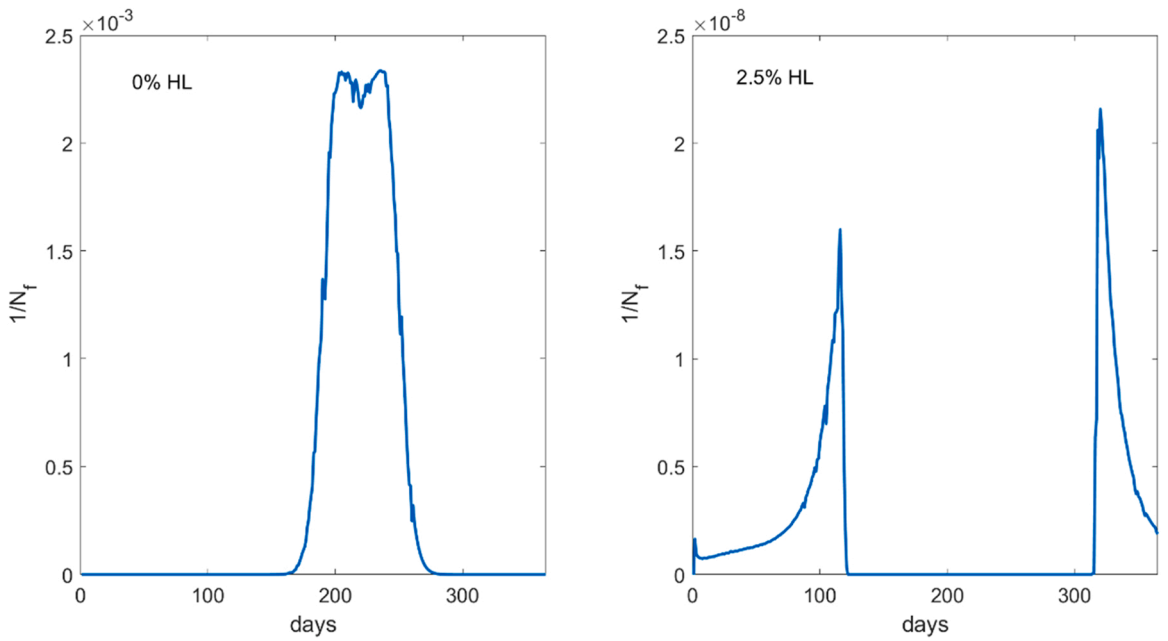

Fig. 17. The calculated fatigue life loss, $1/N_f$, given the strain in year round time.

Data Availability

Data will be made available on request.

References

[1] Y. Sun, C. Du, H. Gong, Y. Li, J. Chen, Effect of temperature field on damage initiation in asphalt pavement: a microstructure-based multiscale finite element method, Mech. Mater. 144 (2020), 103367.
[2] C. Du, Y. Sun, J. Chen, C. Zhou, P. Liu, D. Wang, M. Oeser, Coupled thermomechanical damage behavior analysis of asphalt pavements using a 2D mesostructure-based finite-element method, J. Transp. Eng. Part B: Pavements 147 (2) (2021), 04021012.
[3] D. Lesueur, J. Petit, H.-J. Ritter, The mechanisms of hydrated lime modification of asphalt mixtures: A state-of-the-art review, Roa. Mater. Pavement Des. 14 (1) (2013) 1–16.
[4] S. Bourona, F. Hammouma, H. Ruatb, P. Métaisc, D. Lesueurc, Case study - improving the durability of asphalt mixtures with hydrated lime: field results from highway A84, Case Stud. Constr. Mater. 14 (2021), e00551.
[5] G. Kollaros, E. Kalaitzaki, A. Athanasopoulou, Using hydrated lime in hot mix asphalt mixtures in road construction, Am. J. Eng. Res. 6 (7) (2017) 261–266.
[6] M.M. Iwanski, Effect of hydrated lime on indirect tensile stiffness modulus of asphalt concrete produced in half-warm mix technology, Materials 13 (2020) 4731, https://doi.org/10.3390/ma13214731.
[7] L. Zhou, Y. Sun, Determination of hydrated lime content based on asphalt mastic high temperature performances, E3S Web Conf. 145 (2020) 02029, https://doi.org/10.1051/e3sconf/202014.
[8] W.-J. Zhou, Y. Sun, F.-X. Chi, Q.-L. Cheng, B. Han, Effects of hydrated lime on high-temperature rheological properties of high-viscosity modified asphalt, Adv. Mater. Sci. Eng. 2021 (2021), 4732799-1.
[9] A. Diab, Z.-P. You, A. Othman, H.Y. Ahmed, Fatigue characteristics of hydrated lime modified HMA, Int. J. Pavement Res. Technol. 6 (1) (2013) 31–36.
[10] V.B. Kakad, M.A. Reddy, K.S. Reddy, Effect of aging on fatigue performance of hydrated lime modified bituminous mixes, Constr. Build. Mater. 113 (2016) 1034–1043.
[11] L. Kai, W. Fang, Computer modeling mechanical analysis for asphalt overlay under coupling action of temperature and loads, Procedia Eng. 15 (2011) 5338–5342.
[12] M. Arabania, S.M. Mirabdolazimia, B. Ferdowsib, Modeling the fatigue behaviors of glasphalt mixtures, Sci. Iran. 19 (3) (2012) 341–345.
[13] G. Mazurek, P. Buczynski, M. Iwanski, M. Podsiadło, Thermal analysis-based field validation of the deformation of a recycled base course made with innovative road binder, Materials 14 (2021) 5925, https://doi.org/10.3390/ma14205925.
[14] H. Wu, B. Sun, Z. Li, J. Yu, Characterizing thermal behaviors of various pavement materials and their thermal impacts on ambient environment, J. Clean. Prod. 172 (2018), 1358e1367.
[15] J. Chen, H. Wang, P. Xie, Pavement temperature prediction: theoretical models and critical affecting factors, Appl. Therm. Eng. 158 (2019), 113755.
[16] A.A. Ashaibi, Y. Wang, A. Albayati, J. Byzyka, M. Scholz, L. Weekes, Thermal properties of hydrated lime-modified asphalt concrete and modelling evaluation for their effect on the constructed pavements in service, Sustainability 14 (2022) 7827, https://doi.org/10.3390/su14137827.
[17] SCRB/R9 General specification for roads and bridges, State Corporation of Roads and Bridges, Ministry of Housing and Construction Iraq 2003.
[18] L.-G. Peng, Y.-X. Zhao, H.-R. Zhang, Flexural behavior and durability properties of recycled aggregate concrete (RAC) beams subjected to long-term loading and chloride attacks, Constr. Build. Mater. 277 (2021), 122277.
[19] A.F. Al-Tameemi, Y. Wang, A. Albayati, J. Haynes, Moisture susceptibility and fatigue performance of hydrated lime–modified asphalt concrete: experiment and design application case study, J. Mater. Civ. Eng. 31 (4) (2019), 04019019. rials in Civil Engineering, 28(5): 04015185.
[20] A.F. Al-Tameemi, Y. Wang, A. Albayati, Experimental study of the performance related properties of the asphalt concrete modified with hydrated lime, J. Mater. Civ. Eng. 28 (5) (2016), 04015185.
[21] J. Blazek, G. Sebor, D. Maxa, M. Ajib, H. Paniagua, Effect of hydrated lime addition on properties of asphalt, Pet. Coal 42 (1) (2000) 41–45.
[22] D.N. Little, J.C. Peterson, "Unique effects of hydrated lime filler on the performance-related properties of asphalt cements: Physical and chemical interactions revisited, " J. Mater. Civ. Eng. 17 (2) (2005) 207–218, https://doi.org/10.1061/(ASCE)0899-1561(2005)17:2(207).
[23] Little D.N., Allen D.H., Bhasin A., 2018, Modeling and Design of Flexible Pavements and Materials, Springer International Publishing AG, Switzerland.
[24] M.R. Islam, R.A. Tarefder, Coefficients of thermal contraction and expansion of asphalt concrete in the laboratory, J. Mater. Civ. Eng. Am. Soc. Civ. Eng. 27 (11) (2015) 4015020.
[25] T. Ishikawa, S. Miura, Influence of moving wheel loads on mechanical behavior of submerged granular road bed, Soils Found. 55 (2) (2015) 242–257.
[26] D. Palmer, I. Cole, T. Betts, R. Gottschalg, Interpolating and estimating horizontal diffuse solar irradiation to provide UK-wide coverage: selection of the best performing models Energ., Spec. Issue.: Sol. Photovolt. Trilemma: Effic., Stab. Cost. Reduct., 10, 2017, p. 181.
[27] D. Palmer T. Betts UK-wide Typ. Meteorol. Year Glob. Horiz. Irradiance Data Photovolt. Syst. 2018 doi: 10.17028/rd.lboro.6945311.v1.
[28] Bentz D. (2000), A Computer Model to Predict the Surface Temperature and Time-of-Wetness of Concrete Pavements and Bridge Decks, NIST Interagency/ Internal Report (NISTIR), National Institute of Standards and Technology, Gaithersburg, MD,
[29] Dempsey B.J., Herlache W.A. and Patel A.J., Climatic-Materials-Structural-Pavement Analysis Program. ln Transportation Research Record 1095, TRB, National Research Council, Washington, D.C., 1986, pp. 111–123.
[30] Y. Qin, J.E. Hiller, Modeling the temperature and stress distributions in rigid pavements: Impact of Solar Radiation absorption and heat history development, KSCE J. Civ. Eng. 15 (2011) 1361–1371, https://doi.org/10.1007/s12205-011-1322-6.
[31] J. Busby, UK shallow ground temperatures for ground coupled heat exchangers, Q. J. Eng. Geol. Hydrogeol. 48 (2015) 248–260.
[32] H. Ding, Y. Qiu, A. Rahman, Influence of thermal history on the intermediate and low-temperature reversible aging properties of asphalt binders, Road Mater. Pavement Des. 21 (8) (2020) 2126–2142.
[33] J.P. Planche, D.A. Anderson, G. Gauthier, Y.M. Le Hir, D. Martin, Evaluation of fatigue properties of bituminous binders, Mater. Struct. 37 (5) (2004) 356–359.
[34] Y.D. Wang, B. Behrooz Keshavarzi, Y.R. Kim, Fatigue performance analysis of pavements with RAP using viscoelastic continuum damage theory, KSCE J. Civ. Eng. 22 (6) (2018) 2118–2125.